Available online at www.sciencedirect.com
ScienceDirect
Combustion and Flame 149 (2007) 91–103
Combustion and Flame
www.elsevier.com/locate/combustflame

# Cup-burner flame extinguishment by $CF_3Br$ and $Br_2$

Gregory T. Linteris [a,*], Fumiaki Takahashi [b], Viswanath R. Katta [c]

[a] *Fire Research Division, National Institute of Standards and Technology, Gaithersburg, MD 20899, USA*
[b] *National Center for Space Exploration Research on Fluids and Combustion, NASA Glenn Research Center, 21000 Brookpark Road, Cleveland, OH 44135, USA*
[c] *Innovative Scientific Solutions, Inc., 2766 Indian Ripple Road, Dayton, OH 45440, USA*

Received 9 June 2006; received in revised form 17 November 2006; accepted 9 December 2006

Available online 9 February 2007

**Abstract**

Experiments and calculations have been performed for a methane–air coflow diffusion flame, in the cup-burner configuration, with $CF_3Br$ or $Br_2$ added to the air stream. The time-dependent, two-dimensional numerical code, which includes a detailed kinetic model and diffusive transport, has predicted the flame extinction within 4 or 8% for each. Analysis of the flame structure has allowed the mechanisms of flame weakening in the base and trailing flame regions to be compared. The agents $CF_3Br$ and $Br_2$ behave very similarly with regard to flame extinguishment: both raise the temperature in the flame everywhere, as well as lower radical volume fractions in the trailing diffusion flame and at the peak reactivity spot (the "reaction kernel") at the flame base where the flame is stabilized. The mechanism of lowered radical volume fractions is shown primarily to be due to a catalytic cycle involving bromine species in both regions of the flame, with small contributions from radical trapping by fluorinated species in the trailing diffusion flame. In the reaction kernel, the radical volume fractions are reduced more, and the catalytic radical recombination cycles are shown to be more effective as compared to in the trailing diffusion flame. At the latter location, the effectiveness of the agents is reduced because the hydrocarbon species, which are necessary for the regeneration of HBr, are scarce at the location of the peak radical volume fraction (i.e., at the flame zone), a limitation which does not exist in the reaction kernel, where there is good upstream mixing of the fuel and oxidizer because the base is lifted. That is, the premixed character of the reaction kernel actually allows the HBr in the catalytic cycle to be more effective there because of the effective overlap between the Br and the hydrocarbon species, which allows efficient regeneration of HBr.


*Keywords:* Fire suppression; Cup burner; Halon replacement; Flame extinction; $CF_3Br$

## 1. Introduction

The fire extinguishing agent trifluorobromomethane ($CF_3Br$, Halon 1301) is effective [1] and widely used [2]. Unfortunately, because of its destruction of stratospheric ozone, its production in industrialized nations has been banned [3]. Much recent research has been aimed at finding both short- [4,5] and long-term [6] replacements for $CF_3Br$. As a result, $CF_3Br$ itself has been the continuing subject of many studies [7–13] since an improved understanding of its mechanism of inhibition will help in the search for

* Corresponding author. Fax: +1 (301) 975 4052.
*E-mail address:* linteris@nist.gov (G.T. Linteris).

0010-2180/$ – see front matter 
doi:10.1016/j.combustflame.2006.12.013

alternatives, and nearly all assessments of new agents use $CF_3Br$ as a baseline for comparison of the new agents.

The experimental configurations used to study the inhibition mechanism of $CF_3Br$ have tended to be premixed [14–20] and counterflow diffusion flames [21–24], while a few studies have used flow reactors [25,26]. Premixed flames were used mainly because the overall reaction rate, heat release, and heat and mass transport in these flames can be described with a single fundamental parameter, the laminar burning velocity, and because over certain regions, the flow field can be considered one-dimensional (greatly simplifying data collection and numerical simulations). Similarly, counterflow diffusion flames can be considered one-dimensional along the centerline, and the extinction strain rate has been commonly used as the characteristic suppression parameter. In principle, such fundamental parameters can ultimately be used to relate the behavior of the agent in the laboratory flame to its behavior in suppressing large-scale fires [27]—although this scaling is difficult in practice. For example, under the influence of buoyancy, most common fires become dynamic in nature with large vortical structures which entrain additional surrounding air (and agent) into both the established region and the stabilization region of the flame. Such behavior has been observed in cup-burner flames, for which adding $CF_3H$ to the air stream lifts the flame, and allows the inhibitor to enter the fuel side of the diffusion flame [28].

There have been some experimental studies with $CF_3Br$ in coflow diffusion flames. Creitz [29] determined the blowoff limits with $CH_3Br$ and $CF_3Br$ added to either the fuel or the oxidizer stream for various oxygen volume fractions, and found that oxygen volume fractions approaching 0.30 required over 20% $CF_3Br$ in the oxidizer for flame detachment. Simmons and Wolfhard [30] found the blowoff limits for $CH_3Br$ addition to the fuel and air streams for alkane and hydrogen flames, and showed that blowoff required different amounts of inhibitor for different burner geometries. Their measurements, as well as more recent ones with $CF_3Br$ [31,32], have shown that for jet diffusion flames, lower gas velocities require greater concentrations of inhibitor for extinguishment. Simmons and Wolfhard also performed accompanying spectroscopic measurements in a slot burner with $CH_3Br$ added to the air stream and found enhanced $C_2$ formation as well as a secondary reaction zone (observed via $Br_2$ emission) on the air side with either $CH_3Br$ or ethane and bromine added to the air stream. Despite all the previous work with $CF_3Br$, however, very few fundamental studies have been done with $CF_3Br$ in coflow diffusion flames, and especially in configurations with low-velocity fuel jets (which have structures more closely resembling fires).

The burner selected here is the so-called cup burner [33,34], which is essentially a coflow diffusion flame burner with a wide, low-velocity fuel nozzle rather than the jet nozzle of typical coflow diffusion flames. The cup burner is widely used in the fire protection industry as a scale model flame for testing total-flooding fire suppressants and is the basis of National Fire Protection Association (NFPA) [35] and ISO [36] standards. Typically, the agent is added to the coflowing oxidizer stream and the minimum extinguishing concentration (MEC) is recorded. A vast database exists for the MEC of various fire suppressants with specific fuels (both liquid and gaseous), and these data provide the basis for the minimum design concentration for a particular agent to be used as a fire suppressant. While important research has been done with $CF_3Br$ in cup-burner flames [37,38], the present work goes beyond the previous by providing some new measured parameters (including new data for $Br_2$ addition) and applying detailed numerical modeling to understand the flow field and chemical kinetics important for $CF_3Br$ or $Br_2$ extinguishment of cup-burner flames.

The basic mechanism of halogen flame inhibition was suggested by Rosser et al. [39] and further justified and refined by Butlin and Simmons [40], Dixon-Lewis and co-workers [41,42], Westbrook [19,43,44], and Babushok and co-workers [45]. The reaction mechanism is

$$\mathrm{H}\alpha + \mathrm{X} \rightarrow \mathrm{HX} + \alpha,$$

$$\beta + \mathrm{HX} \rightarrow \mathrm{H}\beta + \mathrm{X},$$

in which X is a halogen, $\alpha$ is a hydrocarbon, and $\beta$ is a reactive radical such as H, O, or OH. Hydrogen atom is typically affected most by the catalytic radical recombination cycles above, and its decrease leads to a lowering of the rate of the chain-branching reaction $H + O_2 \rightarrow OH + O$ and the CO consumption reaction $CO + OH \rightarrow CO_2 + H$. While it is generally believed that the same chemical mechanism is at work in the extinguishment of coflow diffusion flames with added Br compounds, there have been no papers which describe the actual mechanism.

In recent years, numerical investigations [46–48] using detailed chemistry models have revealed the flame structure, blowoff phenomena, and physical and chemical suppression processes for coflow jet diffusion flames. Major findings indicate that the blowoff process is controlled by behavior at the peak reactivity spot (i.e., reaction kernel), formed at the flame attachment point in the edge (base) of diffusion flames. More recently, the extinguishment of cup-burner flames with added inert agents [49] and

$CF_3H$ [28] has been studied. Nonetheless, most of the previous work has been with jet flames, and no cup-burner studies have yet been performed for brominated agents.

The overall objectives of the present study are to understand the physical and chemical processes of cup-burner flame suppression by $CF_3Br$ and $Br_2$ and to provide rigorous testing of the numerical model, which includes detailed chemistry and radiation submodels. This paper describes the experimental and numerical extinguishment limits, as well as the flame structure changes which occur near the limits, for methane as the fuel and $CF_3Br$ or $Br_2$ as the agent.

## 2. Experiment

The burner [34,50], consisted of a cylindrical glass cup (28 mm diameter) positioned inside a glass chimney (53.3 cm tall, 9.5 cm diameter). To provide uniform flow, 6 mm glass beads filled the base of the chimney, and 3 mm glass beads (with two 15.8 mesh/cm screens on top) filled the fuel cup (for gaseous fuels only). Calibrated mass-flow controllers (Sierra 860)[1] provided the gas flow with an uncertainty of 2% of indicated flow. The flow rate of the coflowing gas was held constant at (41.6 ± 0.8) L/min, and the $CF_3Br$ or $Br_2$ was added to that flow. For bromine as the inhibitor, all flow tubes downstream of agent addition as well as the burner base were made of Teflon to avoid reaction. A computer-controlled syringe pump added the liquid $Br_2$ to a 2.1 m long tubing carrying the air, and complete $Br_2$ evaporation was observed to occur within a tubing length of less than 1 m. For determining the extinguishment condition, the agent was added to the air flow (in increments of <1% near extinguishment), and the total flow increased slightly, until liftoff was observed. (For the present flow conditions, the MEC was relatively insensitive to the total flow [28].) The test was repeated at least three times. The coflow oxidizer stream velocity $U_{ox}$ without agent was (10.7 ± 0.21) cm/s, and the fuel jet velocity $U_f$ was (0.921 ± 0.018) cm/s.

The fuel was methane (Matheson UHP, 99.9%), and the air was house compressed air (filtered and dried) which was additionally cleaned by passing it through a 0.01 μm filter, a carbon filter, and a desiccant bed to remove small aerosols, organic vapors, and water vapor. The agents were $Br_2$ (Aldrich, 99.5%) and $CF_3Br$ (Great Lakes).

The flame images for the tests were recorded with video cameras and subsequently digitized. For $CF_3Br$ addition, flame images were captured with a black and white Charge Coupled Device (CCD) video camera (Sony, XC-ST50), and an interference filter (Oriel No. 59295, 430 nm, bandwidth 10 nm) helped to resolve against soot emission and to image CH in the reaction zone [51]. A video frame-grabber board (with a resolution of 640 × 480 and a framing rate of 2 Hz) in a personal computer digitized the images, which were then analyzed to determine the flame base location using the National Aeronautics and Space Administration (NASA) image processing freeware program Spotlight [52]. Thirty images were collected and subsequently analyzed for each flow condition of the flame. Note that in figures which follow, if the uncertainty is shown on the data points, the error bars represent one standard deviation (66% confidence level) in the variation in the flame location for the 30 frames of data (caused by naturally occurring flame flicker).

For the measured parameters, an uncertainty analysis was performed, consisting of calculation of individual uncertainty components and root mean square summation of components. All uncertainties are reported as *expanded uncertainties*: $X \pm ku_c$, using a combined standard uncertainty (estimated standard deviation) $u_c$, and a coverage factor $k = 2$ (95% confidence interval). When reported, the relative uncertainty is $ku_c/X$. The expanded relative uncertainties for the extinguishment volume fraction of $CF_3Br$ and $Br_2$ are 2.7 and 2.0%.

## 3. Numerical model

The unsteady coflow diffusion flames of the cup burner were simulated using a time-dependent, axisymmetric mathematical model known as UNICORN (UNsteady Ignition and COmbustion using ReactioNs) [53]. This model solves $u$- and $v$-momentum equations, continuity equation, and enthalpy- and species-conservation equations on a staggered-grid system. The body-force term from the gravitational field is included in the axial-momentum equation to simulate vertically mounted flames in normal gravity. A clustered mesh system traces the gradients in flow variables near the flame surface. Calculations are made on a physical domain of 200 and 47.5 mm in the axial ($z$) and radial ($r$) directions, with a non-uniform grid system of 251 × 101 or 480 × 384, constructed so that the grid spacing in the flame zone is ≈0.2 or 0.08 mm, respectively, in both the $z$ and $r$ directions. The computational domain is confined by the axis of

[1] Certain commercial equipment, instruments, or materials are identified in this paper for adequately specifying the procedure. Such identification does not imply recommendation or endorsement by NIST, nor does it imply that the materials or equipment are necessarily the best available for the intended use.

symmetry and wall boundaries in the radial direction and by the inflow and outflow boundaries in the axial direction. The outer boundary in the $z$ direction is located sufficiently far from the burner exit (≈15 fuel-cup radii) so that propagation of boundary-induced disturbances into the region of interest is minimal. Flat velocity profiles are imposed at the fuel and air inflow boundaries, while an extrapolation procedure with weighted zero- and first-order terms is used to estimate the flow variables at the outflow boundary. For accurate simulation of the flow structure at the base of the flame, which is very important in flame-extinguishment studies, the fuel-cup wall was treated as a 1 mm long, 1 mm thick tube in the calculations. For simulating the heat transfer between the burner rim and the flame, the temperature of the tubular rim was set at 600 K, which is somewhat higher than the 514 ± 10 K measured previously in the experiments. Since the flames at extinguishment are well lifted from the burner rim, heat losses to the rim, and hence the rim surface temperature, are not as crucial as it would be if our interest were primarily in the flame structure under the normal, stably attached conditions.

The chemical kinetics of the $CF_3Br$- or $Br_2$-inhibited cup-burner flames are described using a detailed chemical kinetic mechanism having 92 species and 1644 elementary-reaction steps, developed by the National Institute of Standards and Technology (NIST) through addition of fluorine- [54,55] and bromine-species [56] inhibition reactions to the GRI-V1.2 methane combustion mechanism [57]. The thermophysical properties such as enthalpy, viscosity, thermal conductivity, and binary molecular diffusion are calculated for each species from the polynomial curve fits developed for the temperature range 300 to 5000 K. Mixture viscosity and thermal conductivity are then estimated using the Wilke and Kee expressions [58], respectively. Molecular diffusion is assumed to be of the binary-diffusion type, and the diffusion velocity of a species is calculated using Fick's law and the effective-diffusion coefficient of that species in the mixture. A simple radiation model based on the optically thin media assumption [59] was incorporated into the energy equation. Only radiation from $CO_2$, $H_2O$, CO, and $CH_4$ was considered in the present study.

## 4. Results and discussion

### 4.1. Flame extinguishment results

The experimental and numerical results (and the discrepancy between the two) for cup-burner flames of methane and air extinguished by pure $CF_3Br$ or $Br_2$ have been presented previously [60]. The numerical code predicts the MEC for $CF_3Br$ to be (2.49 ± 0.01)%, or about 4% higher than the experiment (the uncertainty in the numerical prediction reported here is the change in $CF_3Br$ volume fraction between simulations which caused, or did not cause, flame extinguishment), while the prediction for $Br_2$ is 0.0167, or about 8% higher than the experiment. Similar good predictive ability has been found for, $CF_3H$, $CO_2$, $N_2$, and Ar [60], as well as for $CO_2$ in microgravity [61]. These close results for the simulations with the variety of agents reflect the ability of the code to accurately treat both the complex fluid dynamic stabilization process and the chemical kinetics of the inhibited flame, and provide confidence in the numerically calculated flame structure, to be discussed below.

### 4.2. Flame structure of inhibited and uninhibited flames

The structure of the uninhibited methane–air cup-burner flame in normal gravity has been described previously [49,60,62]. The flames are laminar and nearly axisymmetric. The low fuel and air velocities used in the present investigation yield a weakly strained stable flame that is attached to the burner lip. The heat release in the flame, together with the low flow velocities, promotes buoyancy-induced instabilities outside the flame surface causing it to flicker at a low frequency, as described previously [63]. The computed flame is oscillating at a low frequency with large toroidal vortices forming naturally outside the flame surface. The frequency corresponding to the passage of these vortices [63] (also known as the flame-flickering frequency) is ≈11 Hz, which compares well with the value measured in the experiments (10 to 15 Hz, varying with the coflow oxidizer velocity as described in Ref. [63]).

For flames with $CF_3Br$ or $Br_2$, the inhibitor is added to the air flow (which is held constant), so that the oxidizer velocity increases slightly. As $CF_3Br$ is added, the flame base lifts off of the burner rim and moves inward. At a specific $CF_3Br$ volume fraction, the flame base detaches from the burner, drifts downstream, and does not reattach. (The behavior for $Br_2$ is similar.) For $CF_3Br$, Fig. 1 shows the measured flame base height and radial position for the left and right halves of the flame, as well as that predicted by the numerical calculations. In both the experiment and the calculation, the base oscillation is due to buoyancy-induced flame flicker, and the error bars on the experimental points in Fig. 1 show one standard deviation in the base location. As shown, the flame base height starts at about 0.5 mm with 0% $CF_3Br$, decreases slightly for addition of 1% $CF_3Br$, and then between 1.5 and 2.0% $CF_3Br$ lifts to about 2 mm. The flame ra-

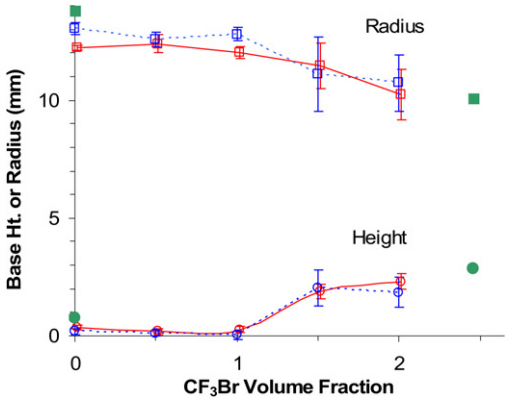


Fig. 1. Measured and calculated flame base radius (□) and height (○) for left (dotted) and right (solid) images of flame base with added $CF_3Br$. The larger solid green symbols at 0 and 2.5% $CF_3Br$ are the model prediction.

dial position also starts to change at a $CF_3Br$ loading of about 1 to 1.5%, at which it moves radially inward by about 2.5 mm. The magnitude of the base oscillation is relatively small up to 1% $CF_3Br$, but above this value, it is about four times larger. The large solid symbols in Fig. 1 show the predicted flame base height and radius. As shown, the numerical prediction is in reasonable agreement with the experiments. The calculated reaction kernel height is about 30% higher for $Br_2$ than for $CF_3Br$.

The flame structure is shown in some detail in Fig. 2 at one instant in the flickering cycle at which the vortex has convected away from the burner and is less influential (i.e., is beyond the distance for which it affects the flow near the reaction kernel). An uninhibited flame is shown in the top frame, while flames with $X_{CF_3Br} = 0.0246$ and $X_{Br_2} = 0.0166$ (i.e., close to extinguishment) are shown in the middle and bottom frames, respectively. The variables include, on the right half, velocity vectors ($\boldsymbol{v}$), isotherms ($T$), total heat-release rate ($\dot{q}$), and the local equivalence ratio ($\phi_{local}$); and on the left half, the total molar flux vectors of atomic hydrogen ($\boldsymbol{M}_H$), oxygen mole fraction ($X_{O_2}$), oxygen consumption rate ($-\hat{\omega}_{O_2}$), and mixture fraction ($\xi$), including stoichiometry ($\xi_{st} = 0.055$). The local equivalence ratio is defined [64] by considering a stoichiometric expression for intermediate species in the mixture to be converted to $CO_2$ and $H_2O$ and is identical to the conventional equivalence ratio in the unburned fuel–air mixture. The mixture fraction was determined by the element mass fractions of carbon, hydrogen, and oxygen as defined by Bilger [65].

In Fig. 2, the common features for the uninhibited flame (top) and the inhibited flames near liftoff (middle and bottom) are as follows. The velocity vectors show the longitudinal acceleration in the hot zone from buoyancy, and as a result of the continuity of the fluid, surrounding air is entrained into the lower part of the flame, inclining the flow streamlines inward due to the low velocity of the fuel flow and the downstream acceleration. Both the heat-release rate and the oxygen-consumption rate contours show a peak reactivity spot (i.e., the reaction kernel [47,64,66]) at the flame base, where the oxygen-rich entrainment flow crosses the flame zone, thus enhancing convective (and diffusive) contributions to the oxygen flux. On the other hand, chain radical species, particularly the H atom, diffuse back against the oxygen-rich incoming flow at the flame base (edge). As a result, chain-branching ($H + O_2 \rightarrow OH + O$) and subsequent exothermic reactions are enhanced particularly at the flame base, thus forming the reaction kernel. In the near-field region shown in Fig. 2, except in the base ($z < 6$ mm) and tip regions, the temperature of the main reaction zone (i.e., the trailing diffusion flame) is 1880 to 1900 K in the uninhibited flame and 1915 to 1930 K with $CF_3Br$, and 1920 to 1970 K with $Br_2$. For the flames in Fig. 2, Table 1 lists the heat-release rate, oxygen consumption rate, velocity, temperature, oxygen mole fraction, local equivalence ratio, and mixture fraction at the reaction kernel. Most of the properties for $CF_3Br$ and $Br_2$ are similar, and these are also similar to those of the uninhibited flame, highlighting the dynamic nature of the reaction kernel, that seeks a location providing a balance between the flow velocity and the reaction rate. It is notable that the temperature at the reaction kernel in the flame inhibited by $CF_3Br$ is 191 K higher than that in the uninhibited flame, whereas the heat-release rate is 18% lower; for flame inhibition by $Br_2$, the temperature in the reaction kernel is 200 K higher and the heat release, 26% lower. As discussed below, the lower heat release at the higher temperature is due to differences in the kinetic rates for radical production in the presence of bromine compounds.

### *4.3. Chemical description of cup-burner flame extinguishment with $CF_3Br$ or $Br_2$*

The structure of the flame base (edge) has been found to be important for understanding the stability of a *jet* diffusion flame [47,64] and of the extinguishment of cup-burner flames by $CF_3H$ [28], and it is likely to be important for the present flames with brominated inhibitors as well. As described above, with 2.46% $CF_3Br$, the reaction kernel is located at a height of 2.84 mm above the burner lip; for 1.67% $Br_2$, it is calculated to be at 4.04 mm. The structure of the flame is investigated in detail at this height, as well as in the trailing diffusion flame at a height 10 mm above the reaction kernel. Since radical concentrations are important for flame stability, Fig. 3

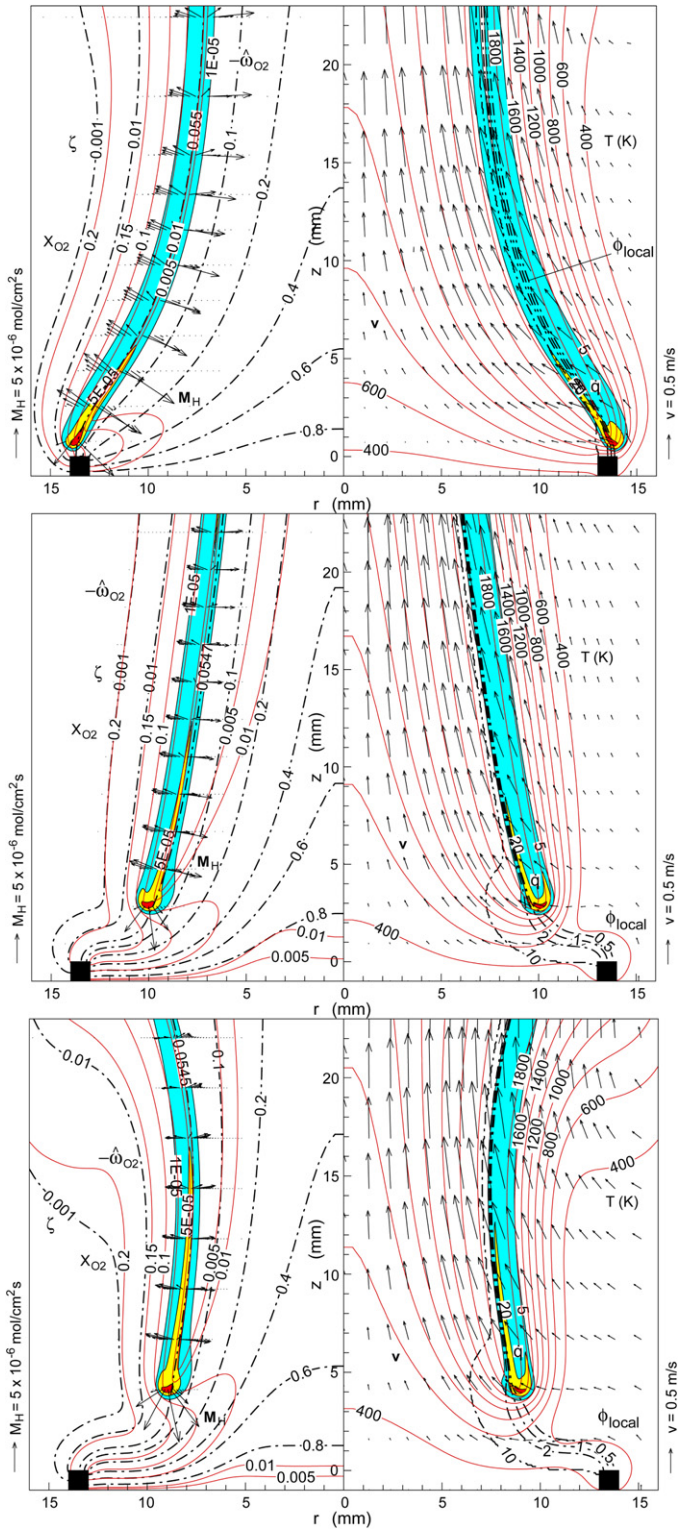


Fig. 2. Calculated structure of methane flames with no agent (top), 2.46% $CF_3Br$ (middle), or 1.66% $Br_2$ (bottom), showing: (right half) velocity vectors, temperature, local equivalence ratio, heat release rate; (left half) $X_{O_2}$, H-atom flux vectors, $-\hat{\omega}_{O_2}$, mixture fraction. ($\dot{q}$ contours: 5, 20, and 80 J cm$^{-3}$ s; $-\hat{\omega}_{O_2}$ contours: $1 \times 10^{-5}$, $5 \times 10^{-5}$, and $2 \times 10^{-4}$ mol cm$^{-3}$ s.)

Table 1
Reaction kernel properties for flames of Fig. 2

| Reaction kernel property | Agent ($i$) | | |
|---|---|---|---|
| | None | $CF_3Br$ | $Br_2$ |
| $X_i$ | 0 | 0.0246 | 0.0166 |
| $\dot{q}_k$ (J cm$^{-3}$ s$^{-1}$) | 155 | 127 | 115 |
| $-\hat{\omega}_{O_2,k}$ (mol cm$^{-3}$ s$^{-1}$) | 0.00041 | 0.00034 | 0.00031 |
| $\lvert \boldsymbol{v}_k \rvert$ (m s$^{-1}$) | 0.275 | 0.260 | 0.332 |
| $T_k$ (K) | 1505 | 1696 | 1705 |
| $X_{O_2,k}$ | 0.041 | 0.041 | 0.044 |
| $\xi_k$ | 0.052 | 0.044 | 0.044 |

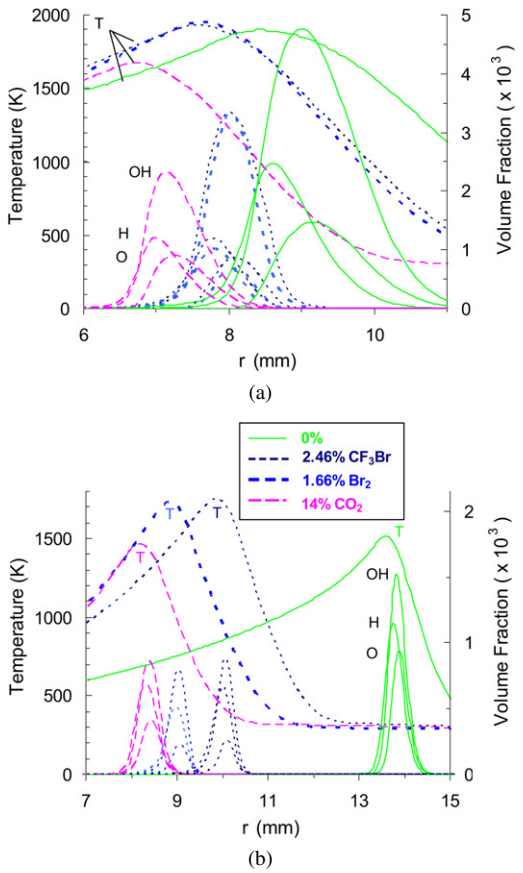


Fig. 3. Flame structures in (a) trailing diffusion flame and (b) reaction kernel regions of a cup-burner flame with 0 and 2.46% $CF_3Br$, 1.66% $Br_2$, or 14% $CO_2$ added to the airflow.

shows the calculated temperature and radical volume fractions as a function of radial location in (a) trailing diffusion flame and (b) reaction kernel. Data are shown for uninhibited flames (solid lines), and those with $X_{Br_2} = 0.0166$ (thick dotted lines) and $X_{CF_3Br} = 0.0246$ (thin dotted lines). For comparison, results are also shown for addition of a physically acting agent ($CO_2$, dashed lines) near the extinguishment limit, $X_{CO_2} = 0.14$ (from [63], Fig. 6, at an elapse time of 0.08 s from the flame-base detachment).

In the trailing diffusion flame (top frame), the most striking features are that the properties for $CF_3Br$ or $Br_2$ addition are very similar, and the net effect from $CO_2$ addition on the radicals is also similar (although the reduction is achieved in a different way). For example, without inhibitor, the peak temperature in the trailing diffusion flame is 1900 K, and the peak volume fractions of OH, H, and O are 0.0047, 0.0024, and 0.0015. The addition of $CO_2$ lowers the peak temperature to 1674 K, whereas the addition of $CF_3Br$ raises it to 1930 K (because of the additional heat release per unit mass of oxidizer from $CF_3Br$ reaction), and the addition of $Br_2$ raises it even more, to 1970 K (because of the higher effective oxidizer volume fraction in the oxidizer stream, since $Br_2$ is an additional oxidizer). Radical volume fractions are reduced comparably with addition of any of the agents: peak [H] and [O] are reduced by about 50% with each of the agents, as is [OH] with $CO_2$ addition, whereas $CF_3Br$ or $Br_2$ addition reduces [OH] by only 30%. In all cases, the radical volume fractions reach their maximum on the air side of the temperature peak, especially for OH and O (because of the hydrocarbon species' inhibiting effect on the chain-branching reactions on the fuel side of the temperature peak).

At the height across the reaction kernel, the effect of the additives on the radicals is again similar, although the reaction kernel location is slightly different. The peak temperatures are significantly lower than in the trailing diffusion flame, 1517, 1465, 1749, and 1730 K, for the uninhibited, $CO_2$, $CF_3Br$, and $Br_2$ flames. In the uninhibited flame, the peak radical volume fractions of OH, H, and O in the reaction kernel are 0.0015, 0.0011, and 0.00095, so that compared with the trailing diffusion flame (height of 10 mm downstream of the reaction kernel), [OH] is about a factor of 3 lower, [H], about a factor of 2 lower, and [O], about the same. Adding the inert agent $CO_2$ (or similar inert agents [60]) lowers the temperature in the reaction kernel only mildly, 52 K (since the reaction kernel moves so as to balance the local reaction rate with the local flow field), as compared to a 232 K decrease in the temperature in the trailing flame. On the other hand, addition of $CF_3Br$ *raises* the reaction kernel temperature by 232 K (and $Br_2$ by 213 K), as compared to a 30 K (50 K for $Br_2$) increase in the temperature in the trailing flame. Nonetheless, radical volume fractions are still reduced in the reaction kernel, although to a slightly smaller degree than in the trailing diffusion flame. For example, [OH] and [H] are reduced about 41% with $CO_2$, $CF_3Br$, or $Br_2$ addition, while and [O] is reduced about 55% with $CO_2$ addition or 72% with $CF_3Br$ or $Br_2$ addition. As in the

trailing diffusion flame, addition of $CF_3Br$ or $Br_2$ has a very similar effect on the radical volume fractions.

Fig. 4 shows the structure of the uninhibited flames (left), or those with $X_{CF_3Br} = 0.0246$ (middle), or $X_{Br_2} = 0.0166$ (right) in the trailing flame (top) or reaction kernel (bottom) region. In all frames (left scale), the reaction flux (i.e., the sum of the local reaction rates in mol $cm^{-3}$ $s^{-1}$) is given for the sum of all hydrocarbon reactions (HC) involving OH, H, and O for the production (+) and consumption (−) of these chain-carrying radicals, as well as the net effect from hydrocarbon reactions ($HC_{net}$). Also shown are corresponding sums for reactions involving halogenated species ($F^+$, $F^-$, and $F_{net}$), and the sum of both the hydrocarbon and the halogen reactions involving those radicals ($Net_{net}$). In all frames (the right scale), the radial profiles of temperature ($T$, K), heat release rate ($Q$, J $cm^{-3}$ $s^{-1}$), and volume fraction ($\times 10^7$) of $CH_4$, $O_2$, and inhibitor ($CF_3Br$ or $Br_2$) are also provided.

In the trailing region of the flame (top frames), the major species volume fractions for the uninhibited case (left frame) are those in a typical diffusion flame. For example, in the top left graph of Fig. 4, the $CH_4$ and $O_2$ are shown to be consumed at a radial location near, but slightly interior to, that of the peak temperature and peak heat release rate. For the inhibited flames (middle and right, top) the $CH_4$ and $O_2$ are again consumed slightly interior to the peak temperature, but heat release occurs throughout the region of radical production.

In the reaction kernel (bottom frames of Fig. 4), the flames have a partially premixed character. There is significant penetration of the oxidizer into the fuel stream, even for the uninhibited flame. With addition of $CF_3Br$, the flame lifts significantly, allowing oxygen levels at the radial location of the branching reactions to reach 3 to 4 times higher than in the trailing part of the flame. The lifted flame also allows the $CF_3Br$ to penetrate into the fuel stream.

The radial distribution of heat release rate is also shown in Fig. 4. For both uninhibited and $CF_3Br$- or $Br_2$-inhibited flames, the peak heat release rate in the trailing flame is about 10 times lower, and has a broader distribution than in the reaction kernel. The heat release rate generally scales with the reaction flux for the radicals (as shown in Fig. 3) for all conditions shown. It is interesting to note that in the trailing diffusion flame, the peak heat release rate per unit volume is about 30% higher with $CF_3Br$ or $Br_2$ than without; whereas, in the reaction kernel (where flame destabilization actually occurs), the addition of $CF_3Br$ or $Br_2$ lowers the peak heat release per unit volume, but only by about 15%.

The effect of $CF_3Br$ on the radicals can be seen through examination of their reaction fluxes. For the trailing region of the uninhibited flames (top left), the hydrocarbon reactions ($HC_{net}$) are net producers of radicals on the oxidizer side of the flame, but net consumers of radicals on the fuel side. With the addition of either $CF_3Br$ or $Br_2$ (top, middle or right), the hydrocarbon reactions are everywhere net producers of radicals, while the reactions with halogen species ($F_{net}$) are everywhere net consumers. For the sum of all reactions ($Net_{net}$), the production of radicals is limited to the central portion of the reaction zone, where mole fractions of *both* the fuel and the inhibitor are low, while the net consumption occurs near the edges of this region, highlighting the effect of $CF_3Br$ or $Br_2$ themselves on the radicals.

For the reaction kernel, Fig. 4 (lower frames) shows that the magnitude of the reaction fluxes (both production and consumption) for radicals is 5 to 8 times higher than in the trailing diffusion flame, despite the lower temperature there (note the scale change on the left ordinate). In the reaction kernel, the radical volume fractions are a few times lower than in the trailing diffusion flame, but they are both produced and consumed at a much higher rate. As discussed previously for other agents [60], this is due to the high rate of chain branching facilitated by the high volume fraction of $O_2$ from the mixing underneath the lifted base. The effect of the brominated species on the radical pool in the reaction kernel (lower, middle and right frames) is again indicated by the reaction fluxes, where reactions with the halogenated species ($F_{net}$) consume radicals which are produced by reactions with the hydrocarbon species ($HC_{net}$). The net effect of all reactions in the region ($Net_{net}$, from reaction with both hydrocarbon and halogen-containing species), however, is a net consumption of radicals. Hence, they must be supplied by diffusion from upper regions (i.e., the trailing diffusion flame), as also indicated in Fig. 2 (bottom left), which shows the high flux of H atoms at the reaction kernel. Since reactions of halogen-containing species with radicals play a key role in weakening the flame base, it is of interest to examine which reactions are responsible.

Fig. 5 shows the reaction flux by radical reaction with halogenated species in more detail. The net reaction flux of chain-carrying radicals (symmetrical about zero flux) is shown by the left scale, while the reaction fluxes for the regeneration steps of HBr from Br are given by the right axis (up from zero). The reaction kernel case (bottom graph) is simpler. For the case of $CF_3Br$ addition, about 84% of the net radical consumption by reaction with halogenated species ($F_{net}$ in Fig. 5, lower left frame) is due to HBr reaction with H or OH (H more important than with OH), and $Br_2$ reaction with H. For the case of $Br_2$ addition, the same reactions are most important for radical con-

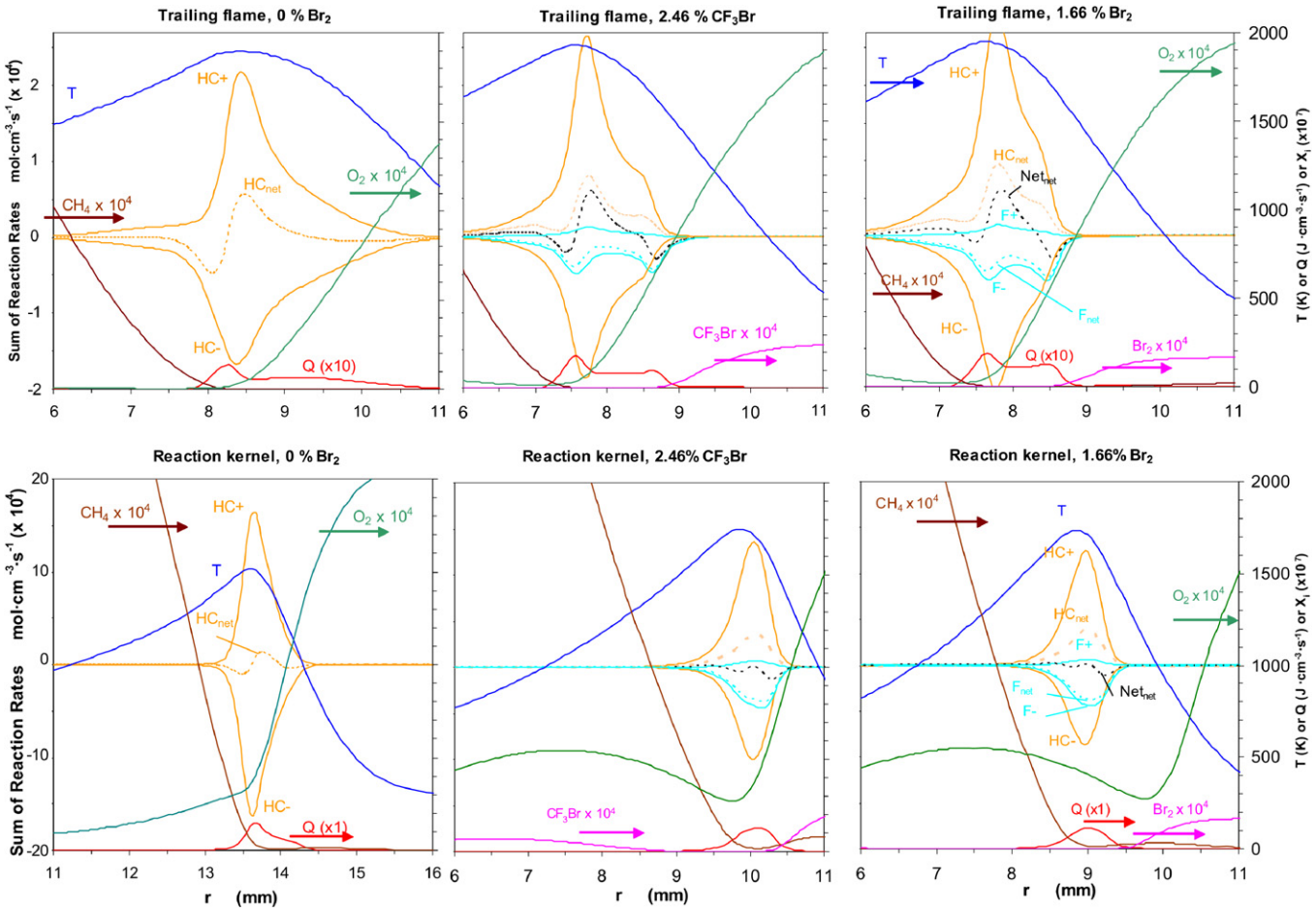


Fig. 4. Sum of reaction rates (left scale) of all reactions involving H, O, or OH, for $CH_4$–air cup-burner flame with no agent (left), 2.46% $CF_3Br$ (middle), or 1.66% $Br_2$ (right). The top frames, trailing diffusion flame; bottom, reaction kernel. Curves are shown for production (+), consumption (−), and the summed (net) effect on radical fluxes, for the halogen (F) and hydrocarbon (HC) reactions. Also shown (using the right scale) are the temperature and heat release, as well as the species volume fraction for $O_2$, $CH_4$, and $CF_3Br$ or $Br_2$ (curve labels in the middle frames are the same as the right frames unless otherwise marked).

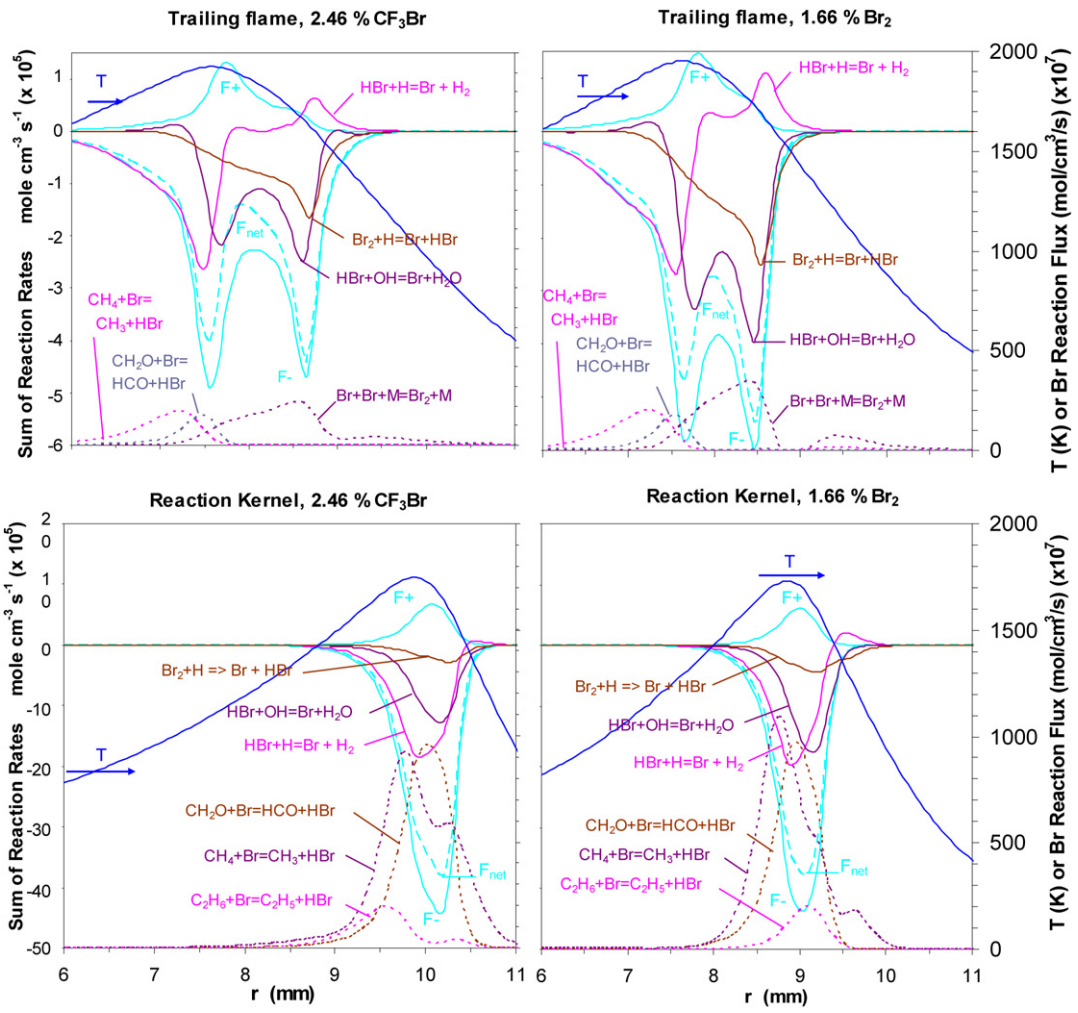


Fig. 5. Detail from Fig. 4 of sum of reaction rates for all reactions involving H, O, or OH, with addition of 2.46% $CF_3Br$ (left frames) or 1.66% $Br_2$ (right frames); top figure, trailing diffusion flame; bottom figure, reaction kernel. For radical consumption, the total is shown for all halogen reactions ($F^-$), as well as the contribution from radical reaction with specific reactions of HBr or $Br_2$. In both flames (top and bottom frames), the important reactions reforming HBr and $Br_2$ are also shown (dotted lines, right scale).

sumption, and account for essentially all of the radical consumption. Thus, for $CF_3Br$ addition, the net contribution to the total halogen radical consumption by the fluorinated species (which includes the important reactions of $CF_3Br$ and $CH_3Br$ with radicals) is only about 15% (in the reaction kernel).

In the trailing diffusion flame with $CF_3Br$ addition (top, left frame), the importance of the bromine reactions to the radical reduction is even stronger. Although not shown in the figure for clarity, one can construct a reaction flux curve for the sum of Br-containing reactions which recombine radicals. That curve is *greater* in magnitude than the net consumption by the sum of *all* halogenated reactions ($F_{net}$); that is, in the trailing diffusion flame, reactions with fluorinated species (as well as those with hydrocarbon species) are net *producers* of radicals, and hence *all* of the consumption comes from reactions with brominated species. In the trailing diffusion flame, HBr + OH is the most important radical recombining reaction, followed by $Br_2$ + H; interestingly, the HBr + H reaction is a net consumer of chain-carrying radicals on the fuel side, but a net producer of them on the oxidizer side of the flame, highlighting the reversible nature of the catalytic cycle.

In the trailing flame (Fig. 5, top frames), there is a large depression in the radical consumption flux curve at a radial position near 8 mm, for either $CF_3Br$ or $Br_2$ addition. To investigate this, we have plotted the reaction rates for the reactions which regenerate the

species (HBr and $Br_2$) necessary for the inhibition cycle. For $CF_3Br$ addition, these reactions,

$$CH_4 + Br = CH_3 + HBr, \quad (1)$$

$$CH_2O + Br = HCO + HBr, \quad (2)$$

$$Br + Br + M = Br_2 + M, \quad (3)$$

$$HBr + H = Br + H_2, \quad (4)$$

are shown (Fig. 5 top, left frame) to occur in regions which exclude the central portion of the radical consumption region: the first two reactions need hydrocarbon fragments, which are present only at the fuel side, and the third reaction needs Br and is favored at lower temperatures, which cause it to be favored on the oxidizer side. The final reaction is only a source of HBr as the temperature decreases on the air side of the peak $T$, and the equilibrium for reaction (4) shifts to the left. The results with $Br_2$ addition are similar. In contrast, in the reaction kernel (Fig. 5, bottom frames), the most important reactions for catalytic species regeneration overlap with the radical location much more effectively than they do in the trailing diffusion flame, and their rates are about twice as fast. Hence, in the reaction kernel, because of the good upstream mixing, the effectiveness of the bromine catalytic cycles is not as limited by the regeneration steps as it is in the trailing diffusion flame. This highlights the suggestion [67] that a key element in a catalytic cycle is the regeneration of the catalytic intermediates. These results are consistent with the finding [68] that the relative performance advantage of $CF_3Br$ over $CO_2$ depends on the flame type, with a lower advantage in counterflow diffusion flames relative to premixed flames. Note that because of the premixing in the reaction kernel where stabilization takes place, cup-burner flame extinguishment is more similar to premixed flame propagation than counterflow diffusion flame extinction, as has been discussed previously [60].

A result of the more effective inhibition in the reaction kernel is that the flame will always be destabilized first at the base (observed in both the calculations and the experiment). This occurs since the catalytic cycles are more effective there, and because the reaction kernel depends on the downstream flame (which has higher radical volume fractions) as a source of radicals via diffusion.

## 5. Conclusions

Cup-burner flames of methane and air with added $CF_3Br$ or $Br_2$ have been studied experimentally and numerically. The numerical code has predicted the flame extinguishment volume fraction within about 4% of experiment value for pure $CF_3Br$, and 8% for $Br_2$. The flame base liftoff has been predicted for $CF_3Br$ within the experimental error. The flame is extinguished by a blowoff process rather than global extinction. With $CF_3Br$ added under near-extinguishing conditions, the flame temperature is higher everywhere as compared to the uninhibited flame, so that any increases in the average heat capacity of the oxidizer is more than offset by heat release from inhibitor reaction.

The chemical details of cup-burner flame extinguishment by $CF_3Br$ or $Br_2$ are strikingly similar. At near-extinguishing $CF_3Br$ or $Br_2$ volume fraction (0.0246 or 0.0167), the cup-burner flame is characterized by two regions: the reaction kernel, which is responsible for stabilizing the flame at the base, and the trailing diffusion flame, which serves as a source of radicals for the reaction kernel. While the volume fraction of chain-carrying radicals (O, H, and OH) is lower in the reaction kernel in the reaction flux of radicals there is a factor of 5 higher, and the heat release rate is also higher (by a factor of 10). $CF_3Br$ or $Br_2$ serves to reduce the radical volume fraction in both regions, although the mechanism differs somewhat. In the reaction kernel, radicals are consumed primarily through a catalytic cycle involving HBr reaction with H or OH, with a small additional contribution from the $CF_3$ fragment. In the trailing diffusion flame, the recombination of radicals is due solely to bromine catalytic cycles, with reactions with fluorinated fragments serving to produce radicals somewhat. In this downstream region of the flame, effective radical recombination is limited by the regeneration steps for HBr in the catalytic cycle which depend on hydrocarbon species, that are scarce at the flame zone (where the peak radical volume fraction is located). As a result, the less efficient catalytic cycle in the trailing diffusion flame reduces the radical volume fractions there somewhat less as compared to the reaction kernel.

## Acknowledgment

This work was supported by the Office of Biological and Physical Research, NASA, Washington, DC.

## References

[1] R.G. Gann, Halogenated Fire Suppressants, ACS Symposium Series, vol. 16, Am. Chem. Soc., Washington, DC, 1975.
[2] S.O. Andersen, Fire J. 81 (3) (1987) 56–62.
[3] P.M. Morrisette, Natural Resources J. 29 (1989) 793–820.

[4] W.L. Grosshandler, R.G. Gann, W.M. Pitts, Evaluation of Alternative In-Flight Fire Suppressants for Full-Scale Testing in Simulated Aircraft Engine Nacelles and Dry Bays, NIST SP 861, National Institute of Standards and Technology, Gaithersburg, MD, 1994.
[5] R.G. Gann, Fire Suppression System Performance of Alternative Agents in Aircraft Engines and Dry Bay Laboratory Simulations, NIST SP 890, vols. I and II, National Institute of Standards and Technology, Gaithersburg, MD, 1995.
[6] R.G. Gann, FY2003 Annual Report—Next Generation Fire Suppression Technology Program (NGP), NIST Technical Note 1457, National Institute of Standards and Technology, Gaithersburg, MD, 2004.
[7] C.R. Casias, J.T. McKinnon, Proc. Combust. Inst. 27 (1998) 2731–2739.
[8] N. Vora, N.M. Laurendeau, Combust. Sci. Technol. 166 (2001) 15–39.
[9] C.H. Kim, O.C. Kwon, G.M. Faeth, J. Propuls. Power 18 (5) (2002) 1059–1067.
[10] Y. Saso, Proc. Combust. Inst. 29 (2003) 337–344.
[11] B.A. Williams, J.W. Fleming, Proc. Combust. Inst. 29 (2003) 345–351.
[12] M. Bundy, A. Hamins, K.Y. Lee, Combust. Flame 133 (3) (2003) 299–310.
[13] K. Seshadri, Combust. Sci. Technol. 177 (5–6) (2005) 871–906.
[14] R.F. Simmons, H.G. Wolfhard, Trans. Faraday Soc. 1 (1955) 1211–1217.
[15] W.E. Wilson, Proc. Combust. Inst. 10 (1965) 47–54.
[16] J.C. Biordi, C.P. Lazzara, J.F. Papp, Proc. Combust. Inst. 14 (1973) 367–381.
[17] K.F. Hayes, W.E. Kaskan, Combust. Flame 24 (3) (1975) 405–407.
[18] H.Y. Safieh, J. Vandooren, P.J. Van Tiggelen, Proc. Combust. Inst. 19 (1982) 117–126.
[19] C.K. Westbrook, Proc. Combust. Inst. 19 (1982) 127–141.
[20] O. Sanogo, J.L. Delfau, R. Akrich, C. Vovelle, J. Chim. Phys. Phys. Chim. Biol. 93 (11–12) (1996) 1939–1957.
[21] T.A. Milne, C.L. Green, D.K. Benson, Combust. Flame 15 (1970) 255–264.
[22] J.H. Kent, F.A. Williams, Effect of $CF_3Br$ on Stagnation-Point Combustion of a Heptane Pool, in: Western States Section Meeting, Combustion Institute, Pittsburgh, PA, 1973, pp. 73–24.
[23] K. Seshadri, F.A. Williams, in: R.G. Gann (Ed.), Halogenated Fire Suppressants, in: ACS Symposium Series, vol. 16, Am. Chem. Soc., Washington, DC, 1975, pp. 149–182.
[24] A. Hamins, D. Trees, K. Seshadri, H.K. Chelliah, Combust. Flame 99 (2) (1994) 221–230.
[25] F. Battin-Leclerc, B. Walravens, G.M. Come, F. Baronnet, O. Sanogo, J.L. Delfau, C. Vovelle, in: A.W. Miziolek, W. Tsang (Eds.), Halon Replacements, 1995, pp. 289–303.
[26] K. Li, E.M. Kennedy, B. Moghtaderi, B.Z. Dlugogorski, Environ. Sci. Technol. 34 (4) (2000) 584–590.
[27] F.A. Williams, J. Fire Flammability 5 (1974) 54–63.
[28] V.R. Katta, F. Takahashi, G.T. Linteris, Combust. Flame 144 (4) (2006) 645–661.
[29] E.C. Creitz, J. Res. Natl. Bureau Standards A Phys. Chem. A 65 (1961) 389–396.
[30] R.F. Simmons, H.G. Wolfhard, Trans. Faraday Soc. 52 (1956) 53–59.
[31] A.R. Masri, Combust. Sci. Technol. 96 (4–6) (1994) 189–212.
[32] A.R. Masri, T.C. Clarke, Combust. Sci. Technol. 105 (4–6) (1995) 345–355.
[33] S.N. Bajpai, J. Fire Flammability 5 (1974) 255–267.
[34] B. Hirst, K. Booth, Fire Technol. 13 (4) (1977) 296–315.
[35] Clean Agent Fire Extinguishing Systems, 2001, NFPA, Quincy, MA, 1999.
[36] Gaseous Fire-Extinguishing Systems Physical Properties and System Design, ISO 14520-Part I, International Organization for Standardization, 2000.
[37] R.S. Sheinson, J.E. Pener-Hahn, D. Indritz, Fire Safety J. 15 (1989) 437–450.
[38] J.L. Lott, S.D. Christian, C.M. Sliepcevich, E.E. Tucker, Fire Technol. 32 (3) (1996) 260–271.
[39] W.A. Rosser, H. Wise, J. Miller, Proc. Combust. Inst. 7 (1959) 175–182.
[40] R.N. Butlin, R.F. Simmons, Combust. Flame 12 (5) (1968) 447–456.
[41] M.J. Day, D.V. Stamp, K. Thompson, G. Dixon-Lewis, Proc. Combust. Inst. 13 (1971) 705–712.
[42] G. Dixon-Lewis, R.J. Simpson, Proc. Combust. Inst. 16 (1977) 1111–1119.
[43] C.K. Westbrook, Combust. Sci. Technol. 34 (1–6) (1983) 201–225.
[44] C.K. Westbrook, Combust. Sci. Technol. 23 (1980) 191–202.
[45] T. Noto, V. Babushok, D.R. Burgess Jr., A. Hamins, W. Tsang, A.W. Miziolek, Proc. Combust. Inst. 26 (1996) 1377–1383.
[46] F. Takahashi, V.R. Katta, Proc. Combust. Inst. 27 (1998) 675–684.
[47] F. Takahashi, V.R. Katta, Proc. Combust. Inst. 28 (2000) 2071–2078.
[48] F. Takahashi, V.R. Katta, Proc. Combust. Inst. 29 (2003) 2509–2518.
[49] F. Takahashi, G.T. Linteris, V.R. Katta, Extinguishment Mechanisms of Cup-Burner Flames, in: 44th Aerospace Sciences Meeting and Exhibit, Reno, NV, AIAA, 2006, Paper No. 2006-0745.
[50] G.T. Linteris, G.W. Gmurczyk, in: R.G. Gann (Ed.), Fire Suppression System Performance of Alternative Agents in Aircraft Engine and Dry Bay Laboratory Simulations, National Institute of Standards and Technology, Gaithersburg, MD, 1995, pp. 201–318.
[51] K.T. Walsh, M.B. Long, M.A. Tanoff, M.D. Smooke, Proc. Combust. Inst. 27 (1998) 615–623.
[52] R. Klimek, T. Wright, Spotlight 1.1, NASA Glenn Research Center, Cleveland, OH, 2002.
[53] W.M. Roquemore, V.R. Katta, J. Visualization 2 (3/4) (2000) 257–272.
[54] D.R. Burgess Jr., www CKMech NIST Mechanisms, http://www.nist.gov/cstl/div836/ckmech/, 1999.

[55] D.R. Burgess, M.R. Zachariah, W. Tsang, P.R. Westmoreland, Prog. Energy Combust. Sci. 21 (6) (1995) 453–529.
[56] V. Babushok, T. Noto, D.R.F. Burgess, A. Hamins, W. Tsang, Combust. Flame 107 (4) (1996) 351–367.
[57] M. Frenklach, H. Wang, C.-L. Yu, M. Goldenberg, C.T. Bowman, R.K. Hanson, D.F. Davidson, E.J. Chang, G.P. Smith, D.M. Golden, W.C. Gardiner, V. Lissianski, GRI-Mech: An Optimized Detailed Chemical Reaction Mechanism for Methane Combustion, Topical Report No. GRI-95/0058, http://www.me.berkeley.edu/gri_mech, The Gas Research Institute, Chicago, IL, 1995.
[58] J.O. Hirschfelder, C.F. Curtis, R.B. Bird, The Molecular Theory of Gases and Liquids, Wiley, New York, 1954.
[59] Computational Submodels, International Workshop on Measurement and Computation of Turbulent Nonpremixed Flames, http://www.ca.sandia.gov/tdf/Workshop/Submodels.html, 2001.
[60] F. Takahashi, G.T. Linteris, V.R. Katta, Proc. Combust. Inst. 31 (2007) 2721–2729.
[61] V.R. Katta, F. Takahashi, G.T. Linteris, Combust. Flame 137 (4) (2004) 506–522.
[62] V.R. Katta, F. Takahashi, G.T. Linteris, Numerical Investigations of $CO_2$ as Fire Suppressing Agent, Fire Safety Science: Proc. of the Seventh Int. Symp., Worchester, MA, Int. Assoc. for Fire Safety Science, Boston, MA, 2003, pp. 531–542.
[63] F. Takahashi, G.T. Linteris, V.R. Katta, Proc. Combust. Inst. 31 (2007) 1575–1582.
[64] F. Takahashi, V.R. Katta, Proc. Combust. Inst. 30 (2005) 375–382.
[65] R.W. Bilger, Proc. Combust. Inst. 22 (1988) 450–488.
[66] F. Takahashi, V.R. Katta, Proc. Combust. Inst. 30 (2005) 383–390.
[67] V.I. Babushok, W. Tsang, G.T. Linteris, D. Reinelt, Combust. Flame 115 (4) (1998) 551–560.
[68] F. Takahashi, G.T. Linteris, V.R. Katta, Experimental and Numerical Evaluation of Gaseous Agents for Suppression Cup-Burner Flames in Low Gravity, in: 7th International Workshop on Microgravity Combustion and Chemically Reacting Systems, NASA, Cleveland, OH, 2003, pp. 277–280.